## Supplementary Information of

# Synthesis of switchable ethyl carbamate selective absorbed intelligent molecularly imprinted polymer and its application in electrochemical sensor analysis

Ming Guo*[a,b], Xinge Zhang[a,b], Yilu Zheng[a,b], Dinghai Huang*[c]

[a] Department of Chemistry, Zhejiang Agricultural & Forestry University, Hangzhou, Zhejiang, 311300, China

[b] National Engineering and Technology Research Center of Wood-based Resources Comprehensive Utilization, Zhejiang Agricultural& Forestry University, Hangzhou, Zhejiang, 311300, China

[c] Department of Polymer Material Science and Engineering, Institute of Advanced Polymer Materials, School of Materials Science and Engineering, Tianjin University, Tianjin 300350,China

The ESI contains: additional results and discussions, supplementary figures, tables.

**Supplementary Experimental**

# S1 Experimental

## S1.1 Synthesis and characterization of DA-MIP

### S1.1.1 Synthesis of Furan-β-CD-CHO

2.0 g silica gel was swollen and dispersed in 50 mL of toluene at 35 °C for 3 h. Then, KH-560 (2 mL) and triethylamine as acid-binding agent (3 drops) was added to the solution. The mixture was purged with a gentle flow of nitrogen gas for 6 min and performed in a water bath at 80°C for 12 h in the presence of nitrogen. The polymer grafted nanoparticles were collected by centrifugation and washed with acetone and methanol respectively for removing additional reagents and solvent. Silica gel-KH-560 was collected by centrifugation and washed with acetone and toluene respectively for removing additional reagents and solvent. The obtained product was dried at 60°C under vacuum condition.

β-CD (10 g) was dissolved in 40 mL of dimethyl sulfoxide in a 100 mL glass flask. 1.61 g of IBX was added into the solution at room temperature for 24 h and filtered. The resultant solution was dropwise added to acetone to form a white precipitation and collected by filtration. This procedure synthesized cyclodextrin aldehyde, which was further freeze-dried. In detail, freshly prepared cyclodextrin aldehyde was dispersed into the mixture of 40 mL dimethyl sulfoxide with 44mL methanol solution. $Al_2O_3$ (0.002 g) and anhydrous $CaCl_2$(0.2 g) was added to the solution, and the mixture was stirred at 50°C for 4 h and filtered. The filtrate freeze-dried to get β-CD-$CH(OMe)_2$.

2g of cyclodextrinacetal and 0.2g of $Na_2CO_3$ were dissolved in 50mL of N, N-dimethylformamide. 0.5 mL of furanyl chloride was added to the solution. The mixture was stirred 12 h at room

temperature, and the resulting white precipitate was filtrated. The resultant solution was further dried in vacuum to get Furan-β-CD-$CH(OMe)_2$. The product and HAc (4 %) was dissolved in dimethyl sulfoxide. After the mixture was stirred 12 h at room temperature, the solution was poured into sodium carbonate aqueous solution to extract the upper oil phase and then poured into a large amount of acetone. The resulting white precipitation was filtrated and freeze-dried to get Furan-β-CD-CHO.

**S1.1.2 Synthesis of molecular imprinted and non-imprinted polymer nanoparticles**

First, furan-β-CD-CHO (5g) and ethyl carbamate (0.5g) were dissolved in 40 mL of dimethylsulfoxide solution. After this mixture had been stirring for 24 h at room temperature, Silica gel-KH-560(2.0 g) and sodium ethoxide (0.6g) were added and stirred at 60°C for 24 h. Then EP (1.17g) was slowly dropped into solution and reacted for 24h at 60°C. After cooling at room temperature, precipitated in acetone (300ml), and washed with hot water and cold water repeated several times to remove unreacted furan-β-CD-CHO. Finally, pure molecularly imprinted polymer powder (MIP) was further dried at 60°C under vacuum.

The molecularly imprinted polymer (5 g) prepared above was continuously fed into 50 mL of dimethyl sulfoxide in a molar ratio of 1.25. Reaction was performed in a water bath at 60°C for 24 h. The solution was filtered when it is still hot. The filter cake was washed three times with aether. The obtained DA-molecularly imprinted polymer (DA-MIP) was dried at 45°C under vacuum condition.

Furthermore, non-imprinted polymer (NMIP) and DA-non-imprinted polymer(DA-NMIP), as a reference, was prepared in the same process without the addition of the template molecule, respectively.

Preparation of rDA1, rDA2 and DA3 as follows:

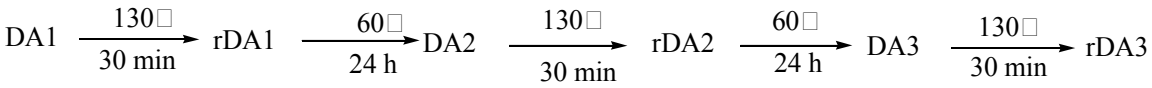


DA1: DA-MIP as the original DA1. rDA1: the DA1 was placed in the oven for 30 min at a temperature of 130°C, and then obtained rDA1 after quenching. rDA2, rDA3 were prepared in the same methods above. DA2: the sample rDA2 was placed in the oven at 60°C for 24 h, and then sample DA2 were obtained after quenching. DA3 was prepared in the same methods as DA2.

## Supplementary discussions

### S2. IR spectra of β-CD, β-CD-CHO and furan-β-CD-CHO

The IR spectra of β-cyclodextrin and its derivatives are shown in Fig.S2.

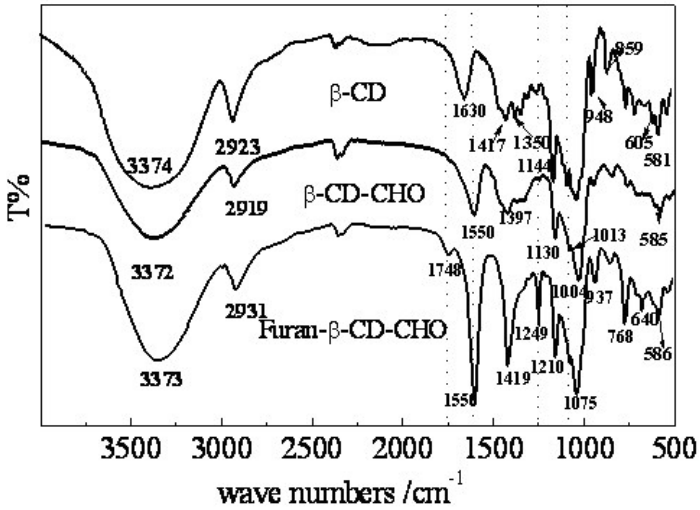


**Figure S2.** FT-IR spectra of β-CD, β-CD-CHO and furan-β-CD-CHO.

Fig.S2 shows the comparison of β-CD, β-CD-CHO and furan-β-CD-CHO in FT-IR. The FT-IR spectrum of β-CD displays a broad peak corresponding to strong absorption at 3374 $cm^{-1}$ which can be ascribed to -O-H stretching vibration [Ref. S1]. At 600 $cm^{-1}$, the peak attributed to -O-H and hydrogen bond bending vibration. Another peak at 2923 $cm^{-1}$ corresponds to C-H stretching vibration of

glucopyranose [Ref. S2]. All these peaks are almost at the same position in comparison with the β-CD-CHO. In β-CD-CHO, a peak at 1748 $cm^{-1}$ is ascribed to C=O stretching vibration.

In the furan-β-CD-CHO, the peaks at 1419 $cm^{-1}$, 1249 $cm^{-1}$ correspond to stretching vibration of furan ring. The asymmetric and symmetric stretching vibration frequencies of C-O-C in the furan ring were 1210 $cm^{-1}$ and 1076 $cm^{-1}$, respectively. Another peak at 1748 $cm^{-1}$ is ascribed to the C=O stretching vibration [Ref. S3].

It can be concluded from the above results that the β-CD-CHO and the furan-β-CD-CHO were successfully synthesized.

**S3. The thermo gravimetric properties of MIP, DA-MIP, β-cyclodextrin and its derivatives**

From Fig.S4a, the weight loss at 150°C in case of silica gel is attributed to the loss of hygroscopic water. The weight loss reached 13% for the modified silica gel in the temperature range of 400-600°C because of introducing organic chemical groups by chemical modification and breaking the regularity of silica gel.

Thermal behavior of MIP shows a two-step weight loss process. The 21% of weight loss in the temperature range of 100-250°C is due to decomposition of cyclodextrin and its derivatives with incomplete reaction in the system. Molecular imprinted polymers are cross-linked to form crosslinked polymers and original structure was destroyed. For these reasons, the thermal gravimetric curve of MIP is located below the modified silica gel.

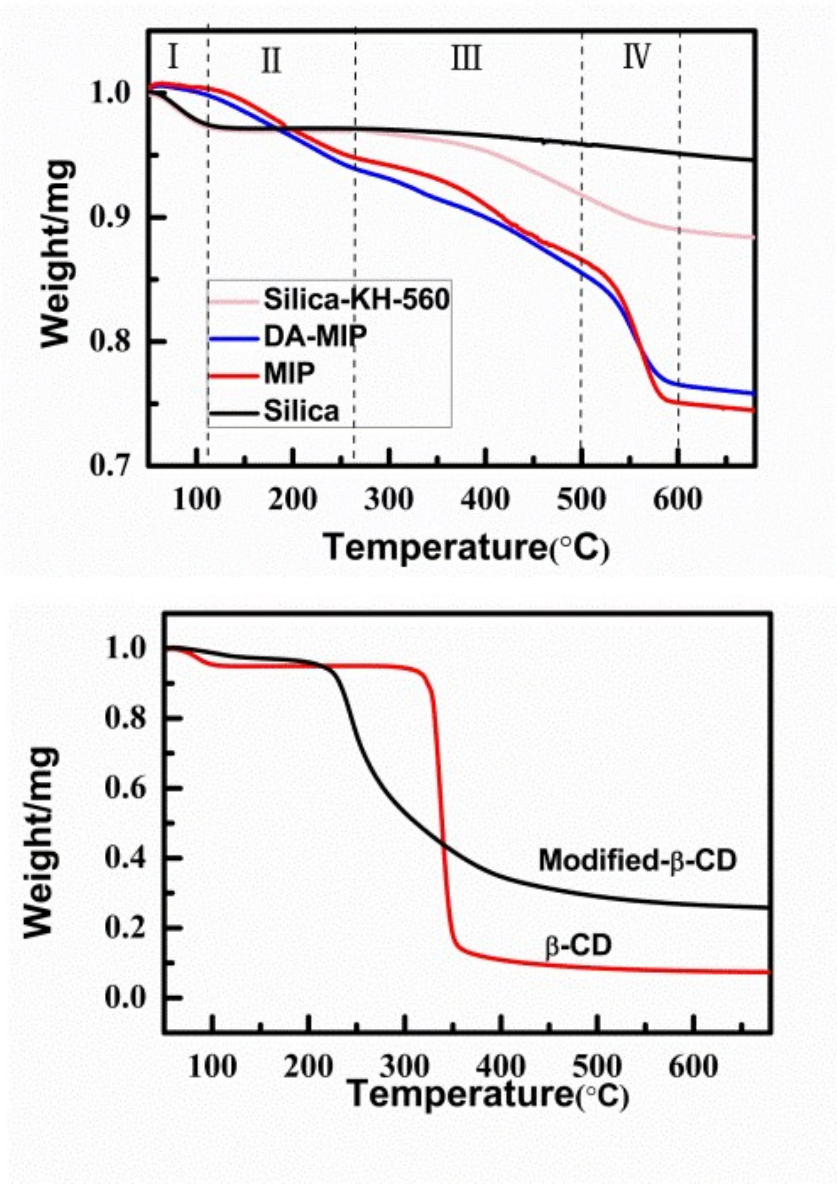


**Figure S4.** TG curve of silica, silica-KH-560, MIP, DA-MIP (a), modified-β-CD and β-CD (b).

Thermal behavior of DA-MIP is similar with MIP. 19% weight loss of its original weight as shown in Fig. S4a, which indicates the thermal stability of DA-MIP is better than that of MIP at above about 600°C, since DA-MIP has a more uniform surface morphology, as evidenced in SEM studies. In a word, there is no significant difference between MIP and DA-MIP, the total weight loss of the two samples is 19%~23% up to 600°C, which indicates that the synthesized polymers have good thermal

properties. Similar thermogravimetric behavior also observed in other Diels-Alder reaction modified polymeric materials. [Ref. S5]

Fig.S4b shows the TG curves of β-cyclodextrin and its derivatives. All of them show loss weight at about 150°C which similar as the case of silica gel and is also attributed to the loss of hygroscopic water. It can be found from Fig.S4b that 89 % of weight loss appears between 300 and 350°C, while 68% of weight loss appears between 250 and 400°C. The results indicate that the decomposition temperature of β-cyclodextrin is higher than that of modified β-cyclodextrin because of the intermolecular hydrogen bond between the β-cyclodextrin and the changed structure after modification.

**S4. The specific absorption and recognition performance of DA-molecularly imprinted polymer**

**S4.1 Standard curve**

Fig.S5 presents the HPLC profiles of EC, BC and MC. All of standard curves are shown in Fig.S6.

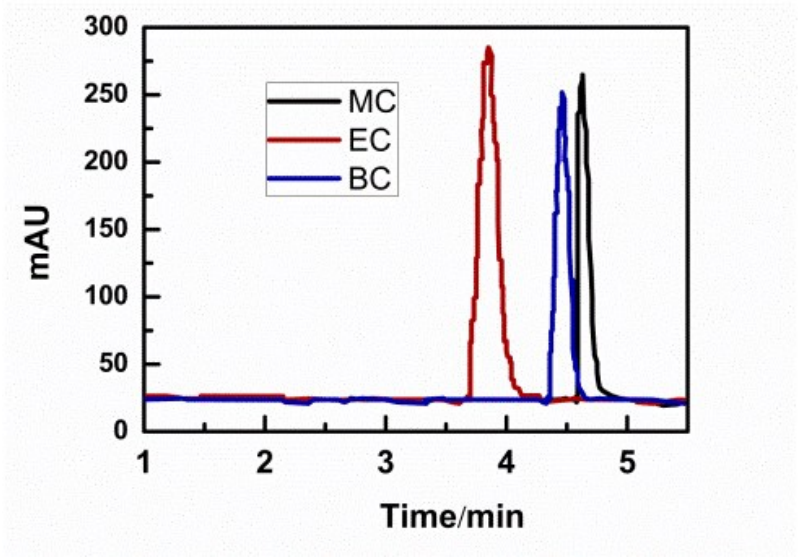


**Figure S5.** The HPLC traces of EC, BCand MC.

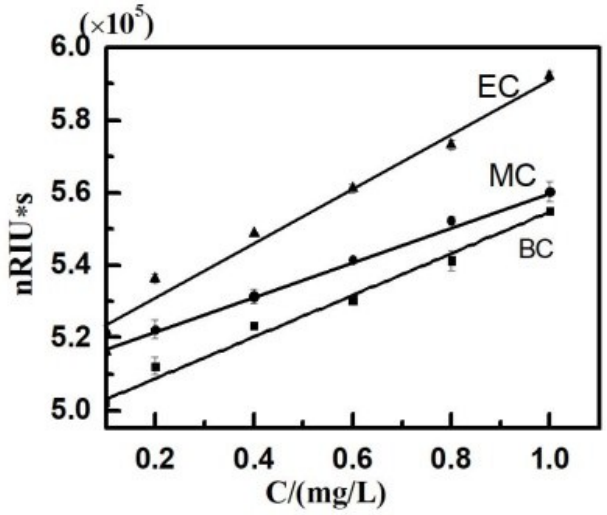


**Figure S6.** The standard curve of EC, BCand MC.

From Fig.S6, it can be seen that the adsorbance increases with increasing of the concentration of the standard. The amount of sample can be determined by comparison to a standard curve.

**S4.2 The absorption kinetics equation**

Fig.S7 shows the time-dependent evolution (according to 2.3(1)) of the EC amount bound by imprinted materials. As can be seen from Fig.S7, the absorption capacity of EC onto MIP and NIP increases with increasing time, and the absorption ability of MIP was better than NMIP, rDA-MIP and DA-MIP.

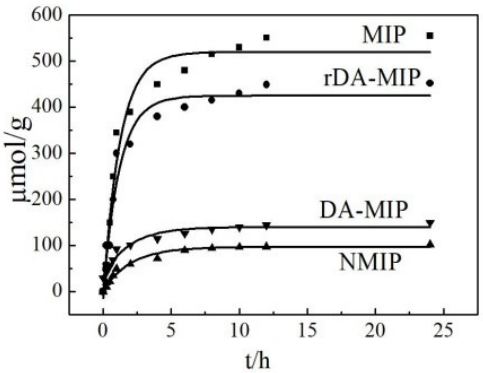


**Figure S7.** The absorption kinetics of MIP, NMIP, rDA-MIP and DA-MIP on EC.

The first stage of absorption kinetics is the instantaneous absorption or external surface absorption. The second step is the gradual absorption stage. The third stage which is the final equilibrium stage due to the extremely low absorptive concentrations left in the solutions and the decrease of absorption sites. Referring to Fig.S7, for MIP and rDA-MIP, the first stage was completed within the first 6 h, and the second stage was then attained; finally the third stage occurred after 8 h. The different stages of the absorption rates observed indicated that the absorption rate was initially faster and then slowed down as the time increased. The absorption behavior of DA-MIP and NMIP in solution of EC was different from that of MIP. The weak absorption capacity of DA-MIP and NMIP in the third stage occurred after 5 h.

**S4.3 Analysis of absorption model of rDA-MIP on ethyl carbamate**

In absorption of template molecules by MIP, it is assumed that the binding of template molecules to binding sites is similar to that of monovalent binding. Therefore, molecules bound to the binding sites can be written as follows:

$$T + M \underset{k_{-1}}{\overset{k_1}{\rightleftharpoons}} TM \quad \text{(S1)}$$

The absorption rate of MIPs for the target molecules varied with time by the following equations:

$$dQ/dt = K_1 c(Q_{max} - Q) - K_{-1} Q \quad \text{(S2)}$$

where $Q$ (μmol·g$^{-1}$) is the amounts of the target molecules adsorbed at time t; $Q_{max}$(μmol·g$^{-1}$) is the apparent maximum binding amount; $C$(μmol·L$^{-1}$) is the concentration of template molecules at time t; $k_1$ is the rate constant of absorption, and $k_2$ is the rate constant of desorption .

When the absorption reaches equilibrium, $dQ/dt = 0$ $K_1/K_2 = K_a$. The absorption model can be written as follows:

$$Qe = \frac{Q_{max} C_e}{1/K_a + C_e} \quad \text{(S3)}$$

Equation (3) can be written as

$$\frac{Q_e}{C_e} = K_a(Q_{max} - Q_e) \quad \text{(S4)}$$

Where $Q_e$ (μmol·g$^{-1}$) are the amounts of the target molecules adsorbed ; $Q_{max}$(μmol·g$^{-1}$) is the apparent maximum binding amount; $C_e$(μmol·L$^{-1}$) are the absorption capacity and concentration at equilibrium; $C$(μmol·L$^{-1}$)-the concentration of template molecules at time t; $K_a$ (L·mol$^{-1}$) is binding constant.

Equation (S4) is the Scatchard equation, the $Q_e/C_e$ for vertical coordinates and the $Q_e$ for abscissa, to make chart.

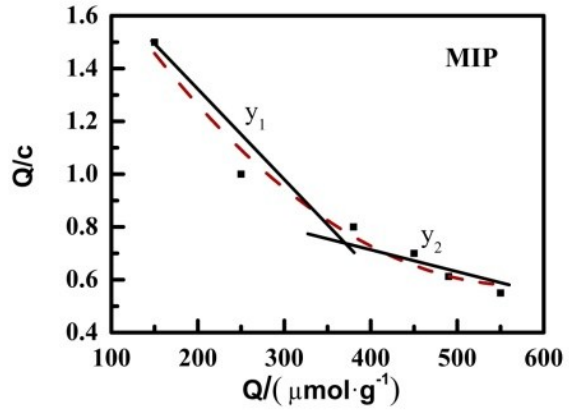


**(a)**

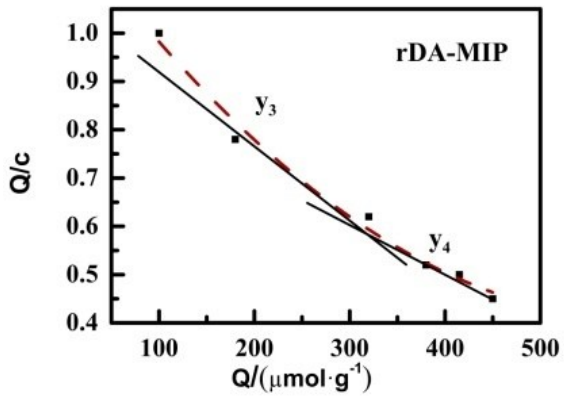


**(b)**

**Figure S8.** The Scatchard absorption model of EC on MIP and rDA-MIP.

As shown in Fig.S8(a), the Scatchard plot for MIP was not a linear curve and consisted of two linear parts with different slopes. It can be seen that the absorption of MIP on EC has two different conditions. In low concentration range, the binding constant ($K_{a1}$) and saturation binding site number ($Q_{max1}$) values were calculated to be $3.3\times10^{-3}$ L·μmol$^{-1}$ and 663.64 μmol·g$^{-1}$, respectively, the slope of the line can be considered high binding constant, which means the specific binding sites of EC. In the high concentration range, the $K_{a2}$ and $Q_{max2}$ values were calculated to be $1.0\times10^{-3}$ L·μmol$^{-1}$ and 1150 μmol·g$^{-1}$, respectively. The slope of the line can be considered low binding constant, which means nonspecific binding sites of EC.

The binding of EC to the rDA-MIP was also analyzed by the Scatchard equation (Fig.S8(b)). The $K_{a3}$ and $Q_{max3}$ values were calculated to be $1.3\times10^{-3}$ L·μmol$^{-1}$ and 776.92 μmol·g$^{-1}$, respectively. The $K_{a4}$ and $Q_{max4}$values were calculated to be $5.7\times10^{-4}$ L·μmol$^{-1}$ and 1298.25 μmol·g$^{-1}$, respectively. Similarly, rDA-MIP has specific binding sites and nonspecific binding sites for EC.

Scatchard absorption model is divided into specific and nonspecific binding sites of two kinds of models, but in fact the specific binding characteristics within the region, nonspecific binding sites also possess certain absorption performance in which specific binding sites have absorption properties. In this paper, Langmuir absorption model equation and Scatchard model are used to compare and analyze.

The nonlinear form of the Langmuir is expressed by the following equations [Ref. S5]:

$$\frac{C_e}{Q_e}=\frac{C_e}{Q_e}+\frac{1}{KQ_{max}} \quad \text{(S5)}$$

where $Q_e$ is the amounts of the target molecules adsorbed (μmol·g$^{-1}$) by MIP, $C_e$ (μmol·L$^{-1}$)the absorption capacity and concentration of EC at equilibrium, $Q_{max}$ is the apparent maximum binding amount (μmol·L$^{-1}$), $K$ is the Langmuir absorption constant (L·μmol$^{-1}$).

The $C_e/Q_e$ for vertical coordinates and the $Q_e$ for abscissa, to make Fig.S9.

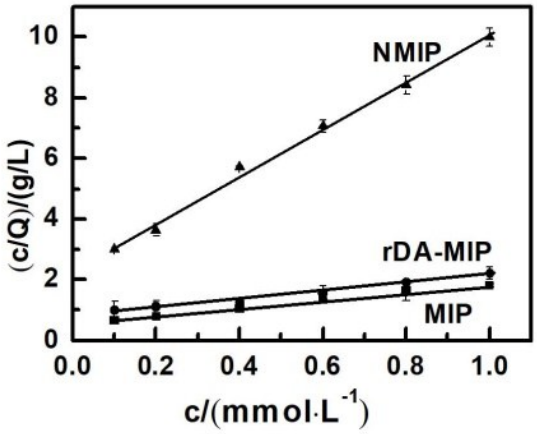


**Figure S9.** The Langmuir model of EC on MIP, NMIP and rDA-MIP.

It can be seen from Fig. S9 that, the binding amount of MIP and rDA-MIP is the amount of the two kinds of binding sites in the Scatchard model. The Langmuir absorption model simulates sorption to the EC. Therefore, compared with Scatchard model, Langmuir absorption model is more reasonable and objective to reflect the binding properties of MIP. NMIP has a good linear relationship with Langmuir absorption model.

**S5. Electrochemical results of DA-molecularly imprinted polymer decorated electrodes**

**S5. 1. The apparent surface area of electrodes**

According to Randles-Sevcik equation(Eq.S3) [S6], the apparent electro-active surface area calculated for modified electrode listed in Table S3($K_3Fe(CN)_6$+0.1 mol·$L^{-1}$KCl, n=1.0,$D_R$=7.60×$10^{-6}$ $cm^2 \cdot s^{-1}$).

$$I_{pa} = (2.69 \times 10^5) n^{3/2} A D_R^{1/2} C_0 V^{1/2} \qquad \text{(S6)}$$

Where $I_{pa}$ is anodic peak current; $A$-the apparent surface area of electrode; $C_0$ is solution concentration;$D_\pi$-diffusion coefficient; V-scan potential.

The results show that the surface area of the modified electrode decreases gradually from a to e, which can explain that the peak current decreases accordingly.

**S5. 2. Electrochemical Impedance Spectroscopy (FRA) of the modified electrodes**

In Fig.S11, the bare-GE (e) AC impedance line is basically a straight line, which is the dominant role of the conductive disperse phase, and the interfacial electron resistance is very small.

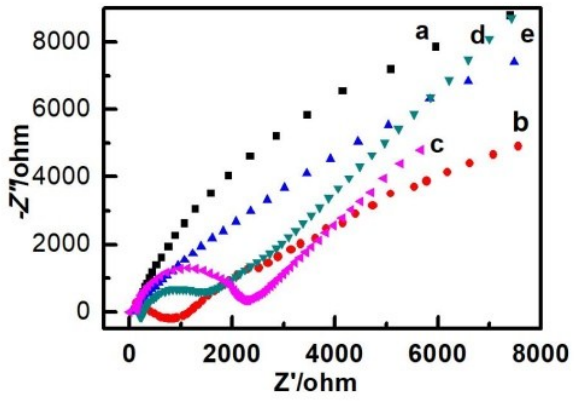


**Figure S11.** The FRA responses at different electrodes in $K_3Fe(CN)_6$+KCl solution. (a) MIP-GE; (b) rDA-MIP-GE; (c) DA-MIP-GE; (d) NMIP-GE; (e) bare-GE.

When NMIP was added into NMIP-GE(Fig.S11d), small-radius curves (small-radius arcs) in the high frequency region indicates that the addition of NMIP made the structure loose and the electron transfer resistance increased. MIP-GE(Fig.S11a) is a straight line, which is caused by the porous structure of the MIP, which makes the surface structure of the electrode loose to form an ion permeable channel. So the electrode resistance becomes smaller, and the electrode response is mainly affected by diffusion. DA-MIP-GE (Fig.S11c), which FRA response is a typical Randles curve, appears in the high frequency region, and in the low frequency region is a straight line, which shows that the response process of the electrode includes the impedance of the charge transfer process and

the diffusion impedance. Because the surface of the electrode structure is compact, the resistance to ion penetration and the resistance of the heterogeneous electron transfer is the strongest. rDA-MIP-GE (Fig.S11b) in high frequency region appears small radius curve shows that electronic transfer resistance is smaller than curve c. The linear part of slope becomes smaller, indicating that the diffusion region resistance becomes large due to the reverse reaction makes imprinting hole exposed. Ion permeable channels opened and reaction is controlled by diffusion mechanism. The results of AC impedance analysis indicate that a new type of imprinted electrode has been successfully prepared.

**S5.3 Equivalent circuit model**

Fitting the AC impedance spectra in Fig.S11 with Zview software can obtain equivalent circuits. Fig. S12 shows that $R_1$ of bare-GE is largest. MIP-GE and rDA-MIP-GE improve the impedance due to increasing surface binding capacity of modified electrode. $R_2$ of bare-GE is minimum. $R_2$ resistance of MIP-GE and rDA-MIP-GE increased significantly, attributed to increasing resistance when $[Fe(CN)_6]^{4-/3-}$ through the electrode surface after modified and reducing diffusion resistance of electrode surface for $[Fe(CN)_6]^{4-/3-}$. The value of n of MIP-GE is the minimum and those of rDA-MIP-GE take second place, maximum for bare-GE, indicating that the electrode surface of MIP is coarse. The R3 values of DA-MIP-GE, NMIP-GE and bare-GE are significantly increased, indicating that all of them have characteristic of Warburg diffusion impedance. And the values of n of the three samples are also large, indicating that the roughness in the three electrodes surface is smaller than MIP-GE and rDA-MIP-GE. The results of the two models are consistent with those of AC impedance analysis.

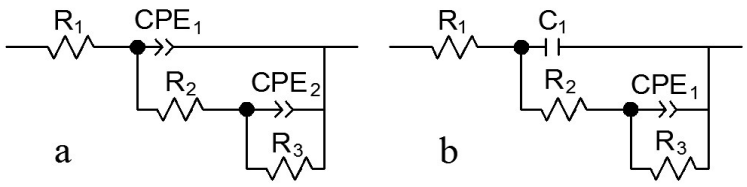

**Figure S12.** The CA responses model of MIP-GE, rDA-MIP-GE and bare-GE (a) and the CA responses model of DA-MIP-GE and NMIP-GE(b).

Where $R_1$ is the solution resistance between the outer surface of the electrode and the reference electrode; $CPE_1$-constant phase elements of double layer capacitance; $CPE_2$ is constant phase element of Faradaic double-layer capacitance; $R_2$ and $R_3$ represent the impedance of electron transfer and the Warburg impedance, respectively; $C_1$-the electric double layer capacitor [Ref. S7].

## S5.4 The relationship between the response current and absorption time

The relationship between the response current of electrochemical sensor and the absorption time was investigated and illustrated in Fig.S13. When the sensor is immersed in EC solution for 8 min, the response current of MIP-GE reaches 85% of the maximum current, both of the MIP and rDA-MIP modified electrodes reach the absorption equilibrium at 15 min. It is shown that the MIP-GE has a high absorption rate, and the addition of MIP makes the electrode surface structure looser, and the specific surface area larger. The specific binding site is determined by the specific absorption capacity of EC. At the same time, the amount of added MIP should be enough to ensure that the electrode has enough imprinting sites, so that the template molecules can easily combine with the specific sites,weaken the mass transfer resistance of the electrode surface, and quickly reach the absorption equilibrium.The current response of rDA-MIP-GE and MIP-GE is essentially the same and the absorption equilibrium is reached after 15 min, which indicates that the absorption capacity is restored after the inverse reaction.

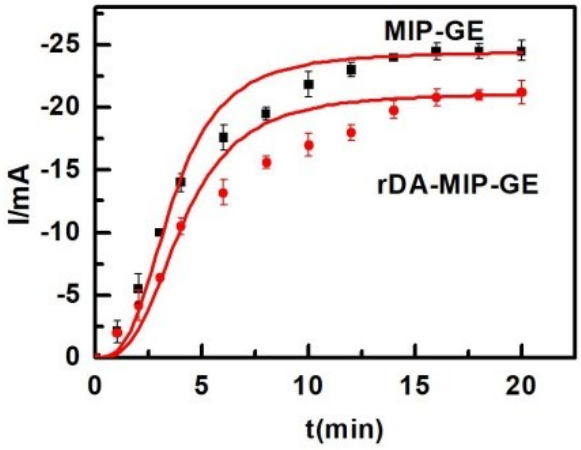


**Figure S13.** The Response current (DPV) versus absorption time for MIP-GE and rDA-MIP-GE in constant EC concentration. ( Scan rate was 0.1 V/s, EC concentration was 1.0 μmol·$L^{-1}$, 0.01 mol·$L^{-1}$ PBS, p H = 7.0).

### S.5.5 Specific Recognition Performance of EC

As demonstrated in Fig.S14, there is no obvious increase with the increase of solution concentration, and the maximum response current is small in DPV response performance of MIP-GE in BC and MC. Although BC and MC have similar chemical structure as EC, the spatial configuration of the EC binding site in MIP does not match for BC and MC. So the two response current do not change significantly, proved that the absorption of MIP-GE on EC with specificity. The weak binding ability of MIP imprinted electrode with BC and MC proved specific absorption of EC on MIP-GE.

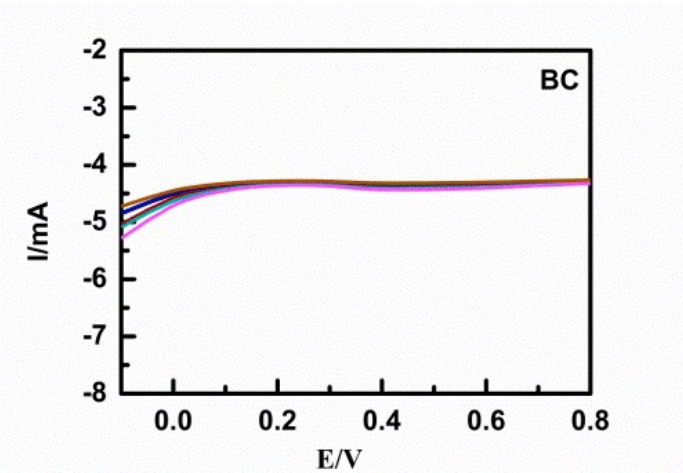

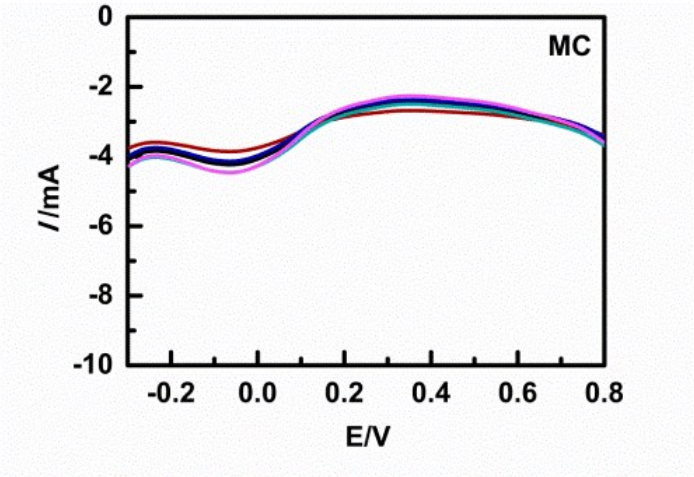


**Figure S14.** The DPV for different modified electrode of BC, MC.

The response performance of modified electrodes to BC and MC is illustrated in Fig.S14. As illustrated in Fig. S15, the maximum current of MIP-GE is 2.5 times of NMIP-GE, 2 times of DA-MIP-GE, and 2.7 times of bare-GE in DPV response performance of MIP-GE in EC solution. Similarly, the maximum response current of rDA-MIP-GE is 2.2 times of NMIP-GE, 1.7 times of DA-MIP-GE and 2.4 times of bare-GE in EC solution. In contrasting, the NMIP-GE and rDA-MIP-GE on the current response in BC and MC solution is basically the same.

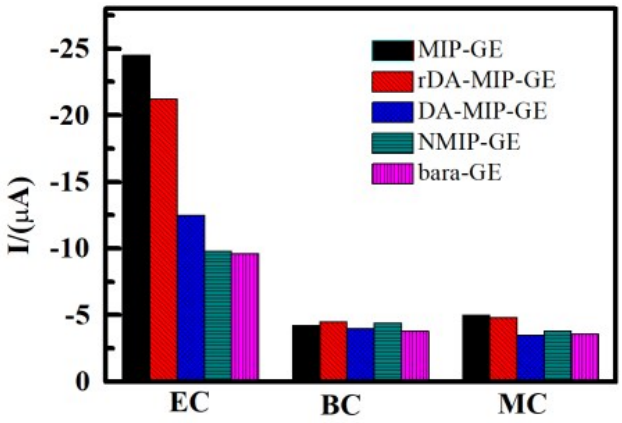


**Figure S15.** The DPV of different modified electrodes to EC, BC, MC, respectively.

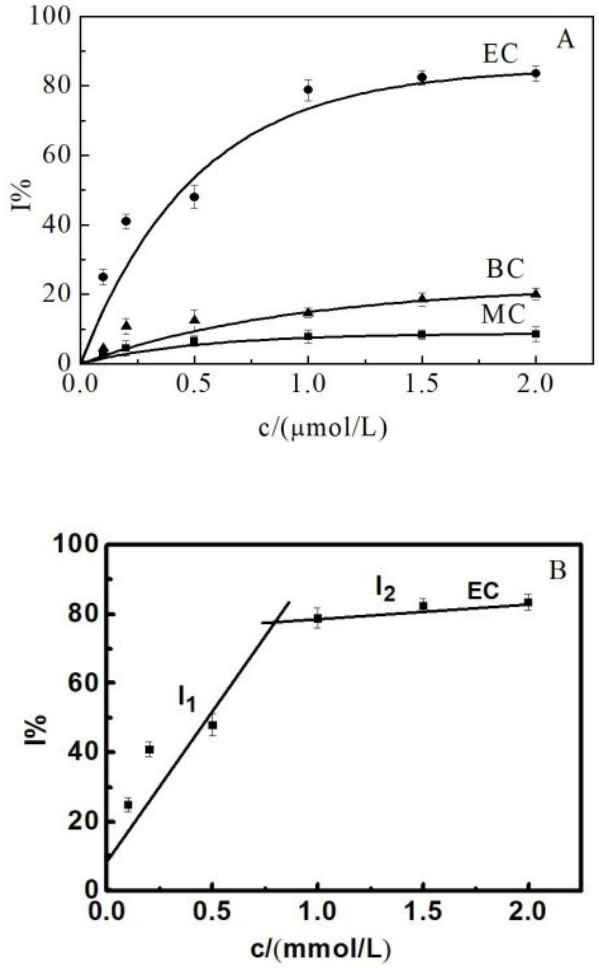


**Figure S16.**The correlation curve between imprinting efficiency and concentrationfor EC, BCand MC, respectively.

In order to investigate the selectivity of imprinted electrodes, the selection capability is expressed by the ratio of current ($I_m / I_n$, $I_m / I_0$, $I_d / I_n$, $I_d / I_0$). The calculated data are listed in Table S4, the results showed that the absorption capacity of MIP-GE to the template molecule is larger. Compared with MIP-GE, the absorption capacity of rDA-MIP-GE decreases slightly. The absorption capacities of EC and MC are both small for MIP-GE and rDA-MIP-GE, indicating that MIP-GE and rDA-MIP-GE have good affinity, specificity and absorption properties for EC and MC.

Fig.S16a shows that the imprinting efficiency is proportional to the concentration of template molecule at low concentration (1.0 μmol·$L^{-1}$or below), while the MIP-GE imprinting efficiency of

template molecules decreases in the range of 1.0 μmol·$L^{-1}$~2.0 μmol·$L^{-1}$. It may because that the template molecule occupies different areas on the electrode surface, and gradually reached saturation. That will influence the surface mass transfer process and the peak current gradually stabilized. The imprinting efficiency of MIP-GE on BC and MC is low. Imprinted efficiency is not change significantly when the concentration changed.

In the range of 0 ~1.0 μmol·$L^{-1}$ and 1.0 ~2.0 μmol·$L^{-1}$, imprinting efficiency showed two different linear relationships for MIP-GE in EC (see Fig. S16b).

Supplement References

S1 Z. M. Feng, Z. L. Zhan, Y. N. Yang, J.S. Jiang, P. C. Zhang, *Bioorg. Chem.* 2017,**74,** 10-14.

S2 P. Li, S. Li, Y. Wang, Y. Zhang, G.Z. Han, *Colloid. Surface. A.*2017, **520,** 26-31.

S3 A. Padwa, A. C. Flick, *Adv. Heterocycl. Chem.* 2013, **110,** 1-41.

S4 C. García-Astrain, A. Gandini,D. Coelho, I. Mondragon, A. Retegi, A. Eceiza, M. A. Corcuera, N. Gabilondo, *Europ. Polym. J.* 2013, **49,** 3998-4007

S5 J. N. Putro, S. P. Santoso, S. Ismadji, Y. H. Ju, *Micropor. Mesopor. Mat.* 2017, **246,** 166-177.

S6 A. J. Bard, L.R. Faulkner, Electrochemical methods: Fundamentals and applications.Wiley, New York 1980.

S7 Y. C. Li, J. Liu, M. H. Liu, F. Yu, L. Zhang, H. Tang, et al. *Electrochem. Comm.* 2016, **64,** 42-45.

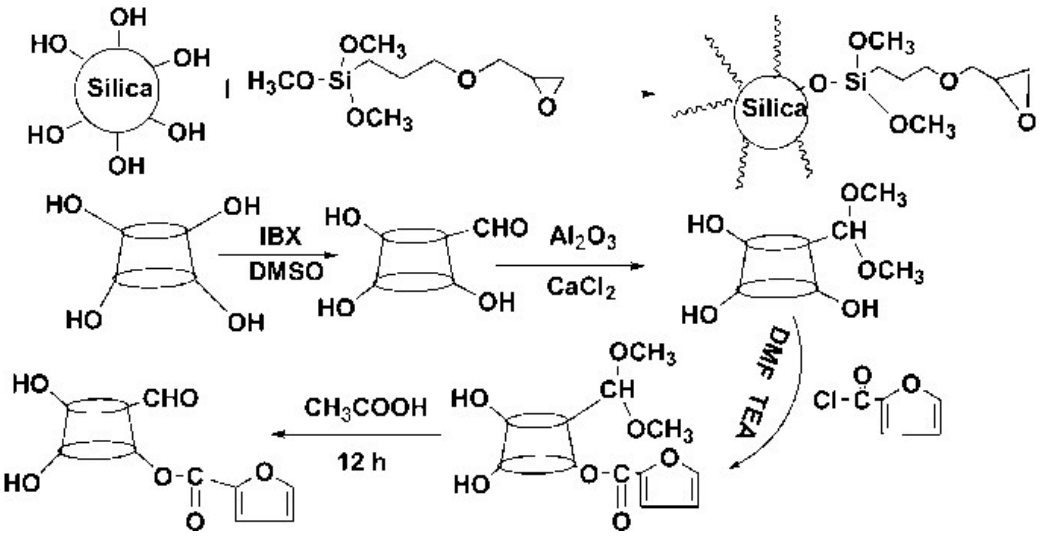


**Figure S1.**The synthetic route of silane grafted silica gel and DA-CD.

**Figure S2.** FT-IR spectra of β-CD, β-CD-CHO and furan-β-CD-CHO.

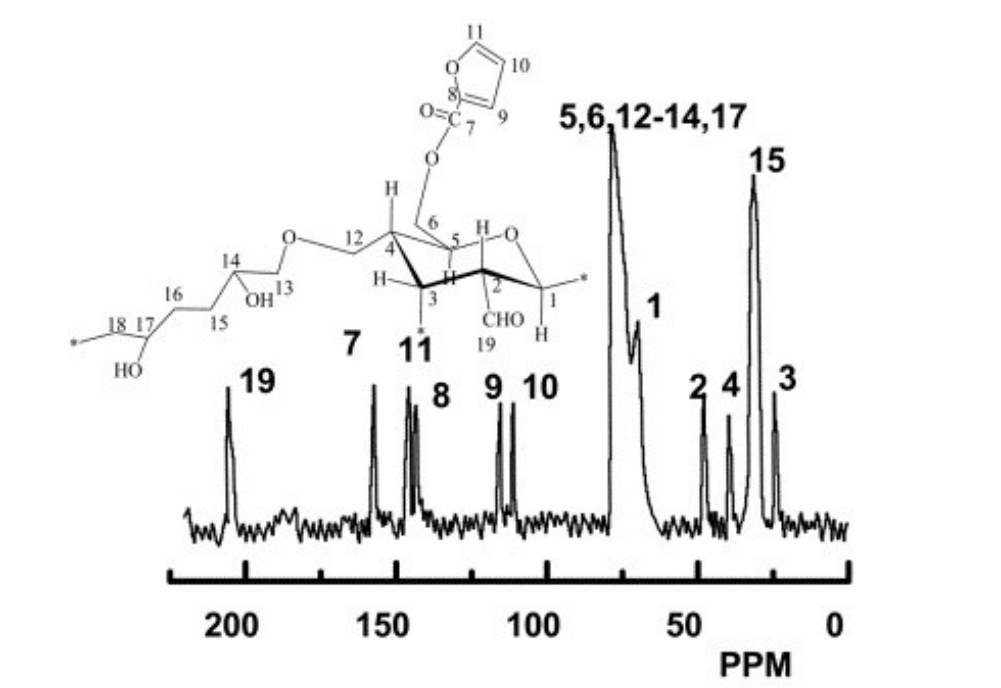


(a) MIP

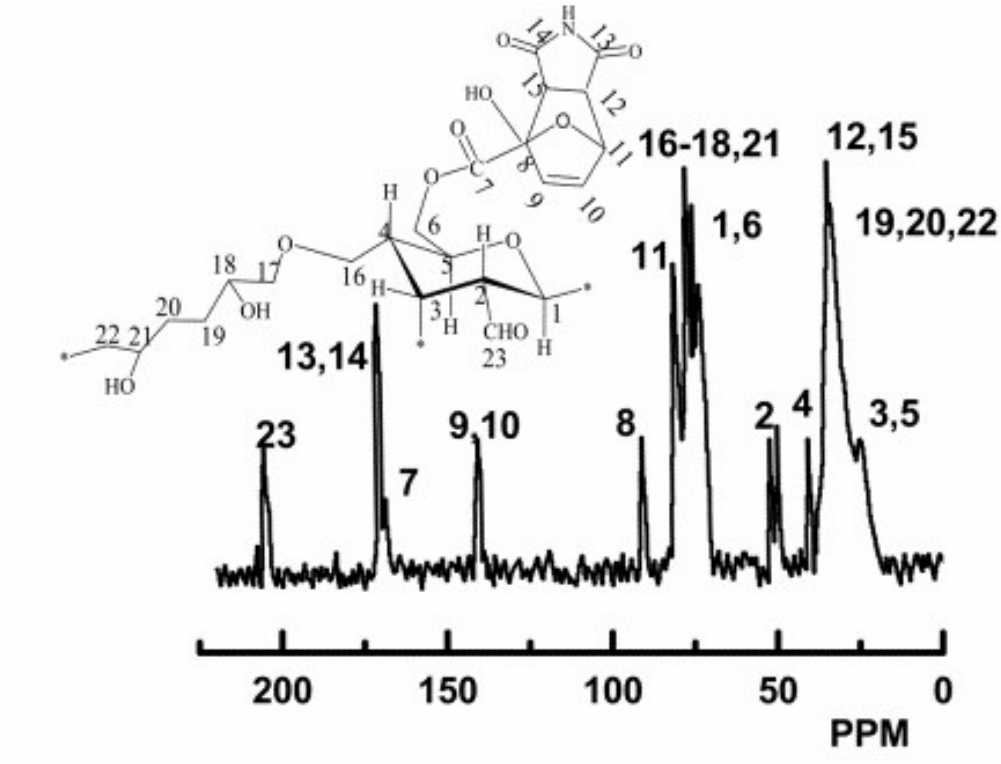


(b) DA-MIP

**Figure S3.**[13]C NMR spectra of (a)MIP, (b) DA-MIP.

**a)**

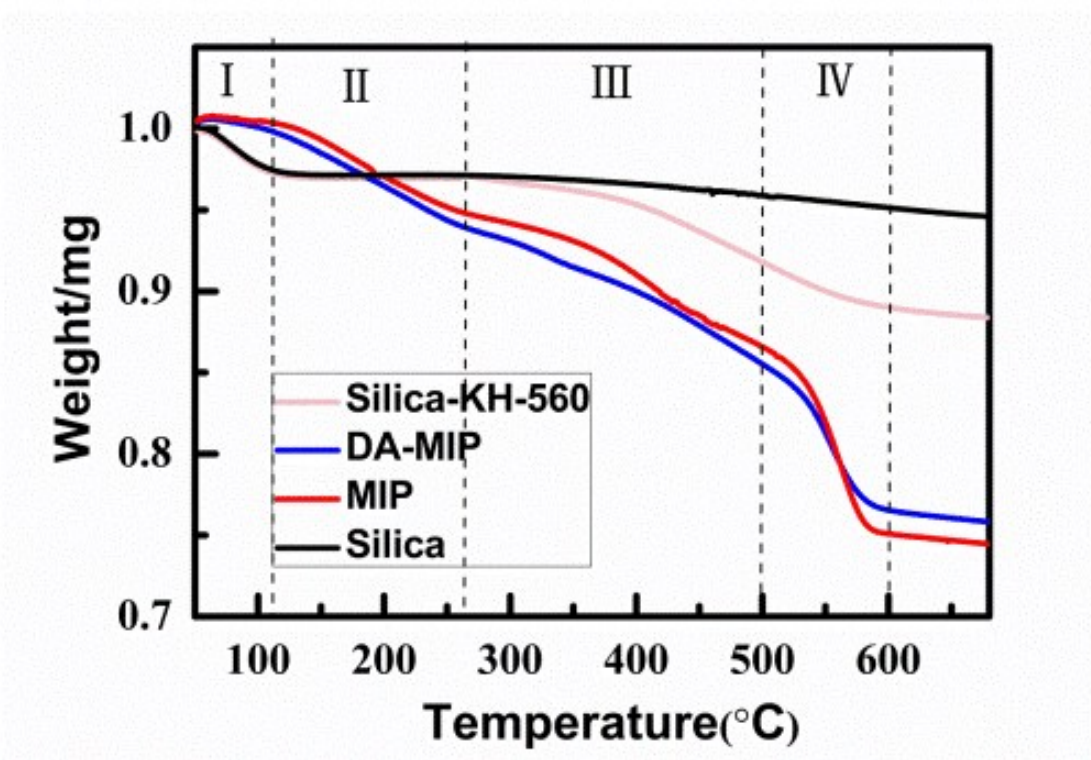


**b)**

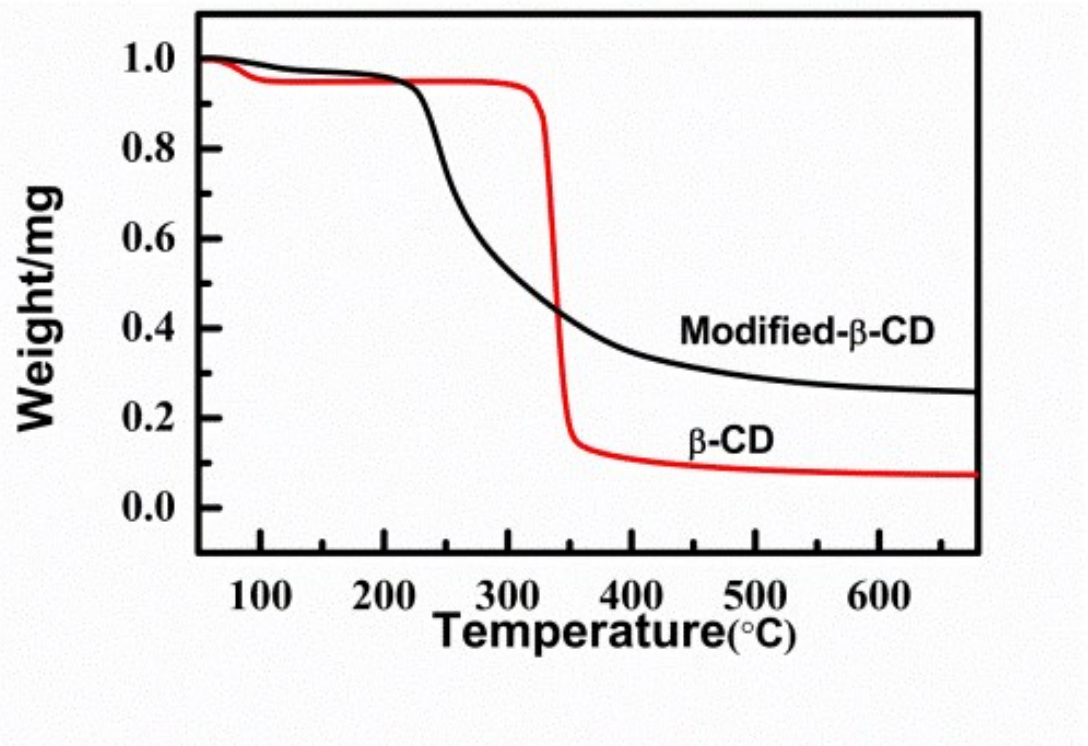


**Figure S4.** TG curve of silica, silica-KH-560, MIP, DA-MIP (a), modified-β-CD and β-CD (b)

**Figure S5.** The HPLC traces of EC, BCand MC.

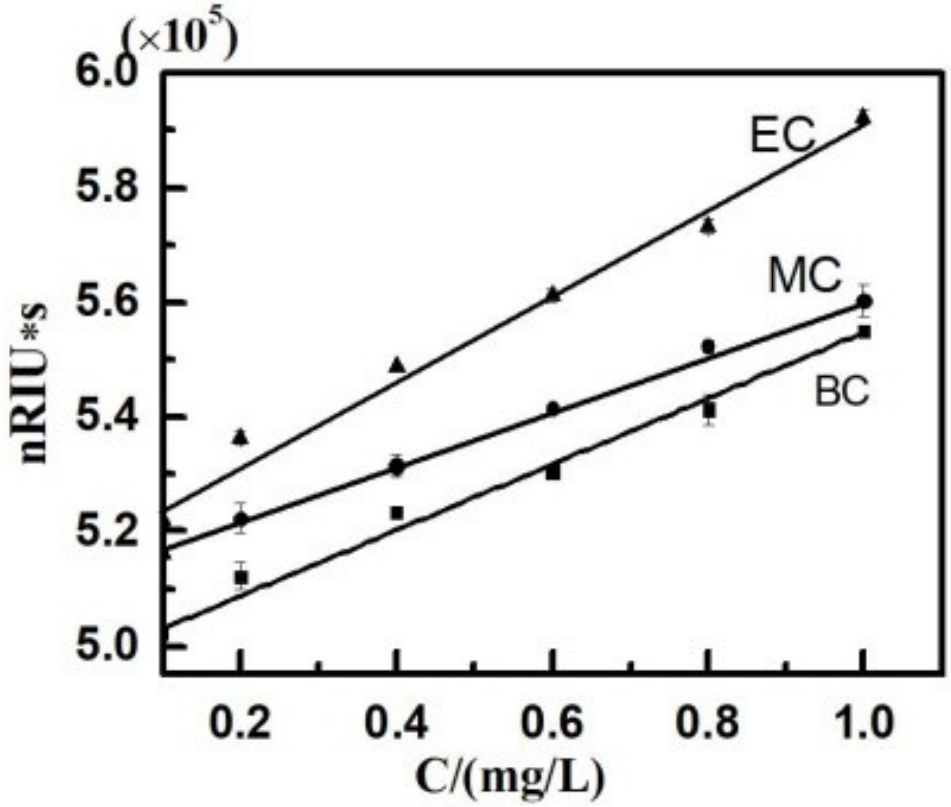


**Figure S6.** The standard curve of EC, BC and MC.

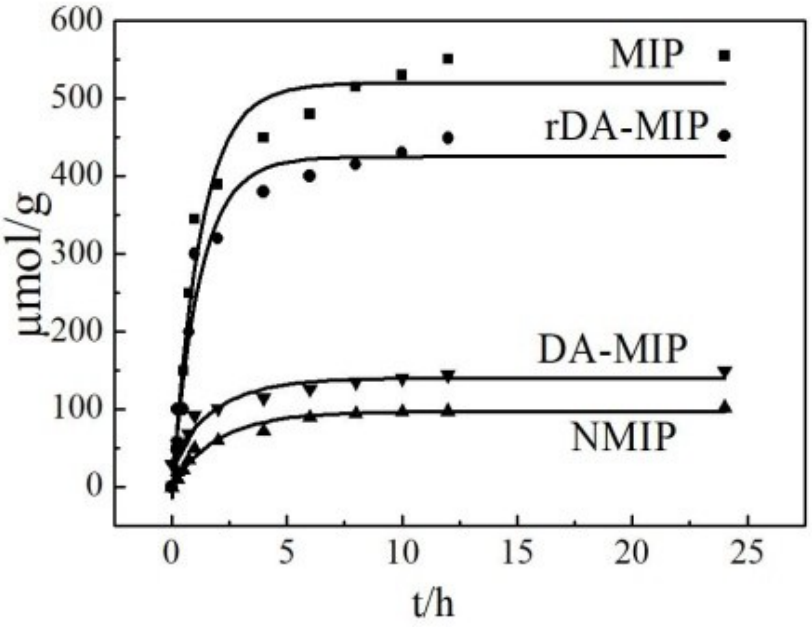


**Figure S7.** The absorption kinetics of MIP, NMIP, rDA-MIP and DA-MIP on EC.

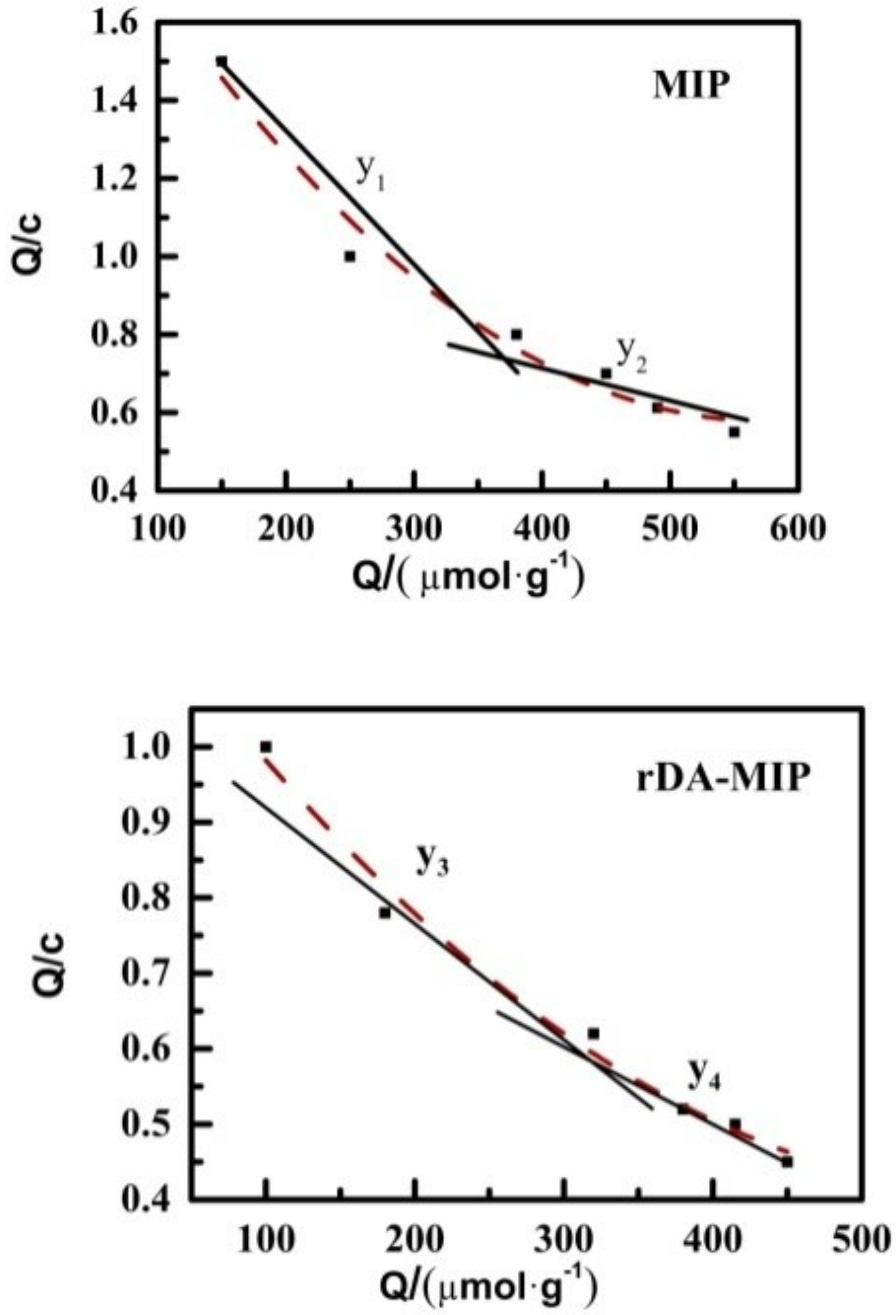


**Figure S8.** The Scatchard absorption model of EC on MIP and rDA-MIP.

**Figure S9.** The Langmuir model of EC on MIP, NMIP and rDA-MIP.

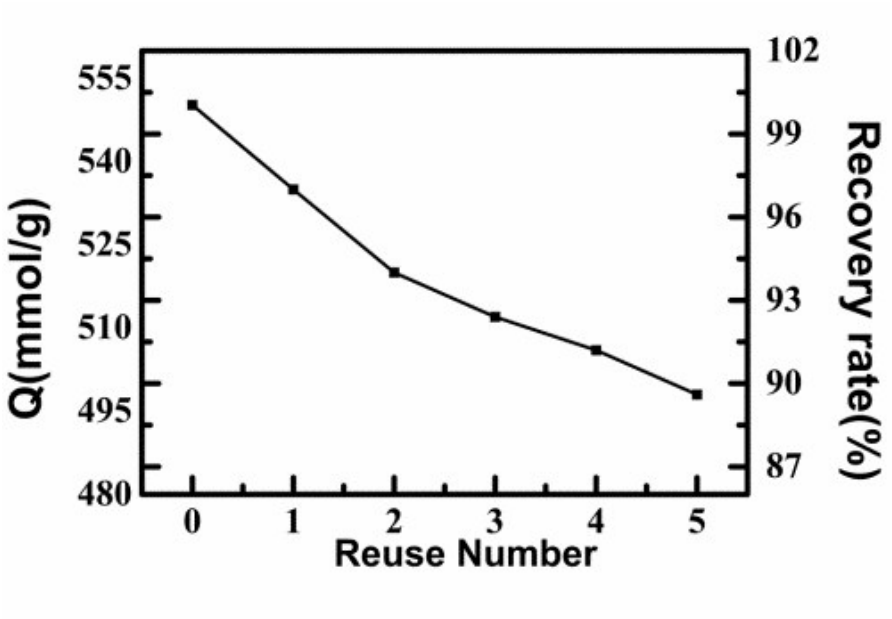


**Figure S10.** Renewable absorption of rDA-MIP on EC.

**Figure S11.** The FRA responses at different electrodes in $K_3Fe(CN)_6$+KCl solution. (a)MIP-GE;(b)rDA-MIP-GE;(c)DA-MIP-GE;(d)NMIP-GE;(e)bare-GE

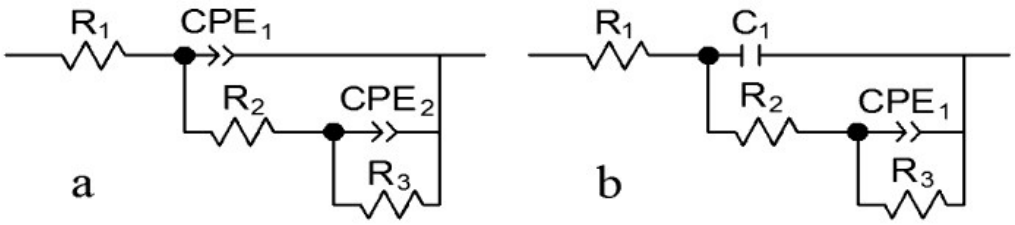


**Figure S12.** The CA responses model of MIP-GE, rDA-MIP-GE and bare-GE (a) and the CA responses model of DA-MIP-GE and NMIP-GE(b)

Where $R_1$ is the solution resistance between the outer surface of the electrode and the reference electrode; $CPE_1$-constant phase elements of double layer capacitance; $CPE_2$ is constant phase element of Faradaic double-layer capacitance; $R_2$ and $R_3$ represent the impedance of electron transfer and the Warburg impedance,respectively; $C_1$the electric double layer capacitor [Ref. S7].

**Figure S13.** The DPV for MIP-GE modified electrode with different adsorption time in 1.0 μmol·$L^{-1}$ initial concentration of EC.

**Figure S14.** The DPV for different modified electrode of BC, MC

**Figure S15.** The DPV of different modified electrodes to EC, BC, MC, respectively.

**Figure S16.** The correlation curve between imprinting efficiency and concentration for EC, BC and MC, respectively.

**Table S1.** Spectral peaks ascription of raw material, intermediates and DA-MIP

| **Functional groups** | **Vibration type** | **Wave number($cm^{-1}$)** | **Functional groups** | **Vibration type** | **Wave number(($cm^{-1}$)** |
|---|---|---|---|---|---|
| -OH | stretching vibration | 3422 | C-H | stretching vibration | 2990 |
| C=C-C=C | conjugated double bond | 2160 | C-O-C | stretching vibration | 1210-1076 |
| Si-OH | Variable angle vibration | 982 | H-O-H | bending vibration | 1630 |
| C=O | stretching vibration | 1722 | Si-OH | stretching vibration | 799 |
| Si-O-Si | stretching vibration | 1150 | Si-O | deformation vibration | 589 |

**Table S2.** $^{13}C$ NMR spectral peaks ascription of MIP and DA-MIP (ppm)

| Material | Peak assignment | chemical shift | Material | Peak assignment | Chemical shift |
|---|---|---|---|---|---|
| MIP | C6 | 79.2 | MIP | C19 | 203.1 |
| MIP | C12- C14 | 76.5 | DA-MIP | C8 | 90.0 |
| MIP | C7 | 158.5 | DA-MIP | C9，C10 | 140.0 |
| MIP | C8 | 141.1 | DA-MIP | C11 | 79.4 |
| MIP | C9 | 110.4 | DA-MIP | C12 | 35.5 |
| MIP | C10 | 116.6 | DA-MIP | C13，C14 | 169.6 |
| MIP | C11 | 145.5 | DA-MIP | C15 | 32.3 |

**Table S3.** The apparent surface area (A) and other parameters of Randles–Sevcik equation.

| | MIP-GE | rDA-MIP-GE | DA-MIP-GE | NMIP-GE | bare-GE |
|---|---|---|---|---|---|
| n | 1 | 1 | 1 | 1 | 1 |
| $D_R$ | $7.60\times10^{-6}$ | $7.60\times10^{-6}$ | $7.60\times10^{-6}$ | $7.60\times10^{-6}$ | $7.60\times10^{-6}$ |
| A | 0.4902 | 0.4505 | 0.2391 | 0.1225 | 0.1132 |

**Table S4.** The Current ratio of MIP-GE and rDA-MIP-GE on EC, BC, MC.

| **Substrates** | **Ratio** | | | |
|---|---|---|---|---|
| | **$I_m/I_n$** | **$I_m/I_0$** | **$I_d/I_n$** | **$I_d/I_0$** |
| EC | 2.52 | 2.54 | 2.12 | 2.14 |
| BC | 1.02 | 1.05 | 1.05 | 1.07 |
| MC | 1.28 | 1.34 | 1.25 | 1.32 |

Where $I_m$-EC, BC, MC current on MIP-GE; $I_n$ is -EC, BC, MC current on NMIP-GE; $I_d$ represent EC, BC, MC current on rDA-MIP-GE;$I_0$-EC, BC, MC current on bare-GE.